Complementary functions of ATM and H2AX in development and suppression of genomic instability

Shan Zha, JoAnn Sekiguchi*, James W. Brush, Craig H. Bassing†, and Frederick W. Alt‡

Howard Hughes Medical Institute, Children's Hospital, Immune Disease Institute, and Department of Genetics, Harvard Medical School, Boston, MA 02115

Contributed by Frederick W. Alt, April 11, 2008 (sent for review March 22, 2008)

Upon DNA damage, histone H2AX is phosphorylated by ataxia-telangiectasia mutated (ATM) and other phosphoinositide 3-kinase-related protein kinases. To elucidate further the potential overlapping and unique functions of ATM and H2AX, we asked whether they have synergistic functions in the development and maintenance of genomic stability by inactivating both genes in mouse germ line. Combined ATM/H2AX deficiency caused embryonic lethality and dramatic cellular genomic instability. Mechanistically, severe genomic instability in the double-deficient cells is associated with a requirement for H2AX to repair oxidative DNA damage resulting from ATM deficiency. We discuss these findings in the context of synergies between ATM and other repair factors.

DNA repair | embryonic lethality | oxidative DNA damage

DNA double-strand breaks (DSBs) can result from normal cellular metabolism, exogenous DNA-damaging agents, or as programmed events during lymphocyte development. Because unrepaired and misrepaired DSBs can lead to cell death or transformation, a complex protein network has evolved to monitor them and lead to their repair. Ataxia-telangiectasia mutated (ATM) is a member of the phosphoinositide 3-kinase-related protein kinase (PIKK) family, which also includes the DNA-dependent protein kinase (DNA-PK) and ataxia–telangiectasia and Rad3-related kinase (ATR). ATM is activated immediately upon DSBs and acts as a master regulator of the DSB response by phosphorylating a host of downstream proteins, including repair factors and checkpoint proteins, such as p53. Thus, ATM-deficient cells have DNA repair defects; spontaneous genomic instability; hyperradiosensitivity; defects in G_1/S, intra-S, and G_2/M checkpoints; and compromised p53-mediated apoptosis. Consequently, Atm-deficient mice are predisposed to thymic lymphomas with clonal translocations (1–4). In addition, ATM also suppresses the accumulation of intracellular reactive oxygen species (ROS) (5–7). Correspondingly, antioxidant treatment significantly delays thymic lymphoma onset in Atm-deficient mice (8, 9), suggesting that increased ROS levels contribute to lymphomagenesis in the ATM-deficient background.

ATM rapidly phosphorylates histone H2AX, a mammalian histone H2A variant, on its carboxyl-terminal SQE motif to generate "γ-H2AX" over large chromatin domains flanking DSBs (10). ATM also phosphorylates other DSB response proteins including MDC1, 53BP1, and NBS1, which bind γ-H2AX to form macromolecular complexes (foci) (11). Deficiency for H2AX or other DSB response proteins leads to a subset of ATM-deficient phenotypes, including genomic instability, DNA repair defects, and radiosensitivity (11, 12), potentially reflecting their role as ATM substrates. However, H2AX-deficient cells have largely normal G_1/S and intra-S checkpoints and p53-mediated apoptosis (13), reflecting H2AX-independent ATM functions. In this context, although thymic lymphomas with clonal translocations are common in an ATM-deficient background, they are rare in the H2AX-deficient background unless p53 is also eliminated (14, 15). However, H2AX can be phosphorylated by DNA-PK and, potentially ATR in response to replication-related DNA damage, implying ATM-independent functions of H2AX (16–18). Spontaneous genomic abnormalities observed in metaphases of H2AX-deficient B cells are about equally divided between chromosome and chromatid breaks, whereas those from ATM-deficient B cells are mainly chromosome breaks (19). Because chromosome breaks mainly derive from prereplication lesions, whereas chromatid breaks generally represent postreplication lesions, H2AX may have postreplication repair functions distinct from those of ATM. Thus, although H2AX is an ATM substrate, H2AX and ATM likely have independent functions that theoretically could synergize in DNA repair and maintenance of genomic integrity.

Although ATM is not required during embryonic development, ATM deficiency has synergistic impacts on deficiencies for several DNA repair factors, among them poly(ADP-ribose)polymerase (PARP) 1/2 and DNA ligase IV (20, 21). Double deficiency for ATM and PARP1/2 leads to embryonic lethality, which is thought to result potentially from severe genomic instability (20). Although ATM deficiency actually rescued the neuronal apoptosis and late embryonic lethality of ligase IV-deficient mice, likely via its role in eliminating p53-dependent apoptosis in neuronal cells, mouse embryonic fibroblasts (MEFs) that lack both ATM and ligase IV displayed severe growth defects and more severe genomic instability than MEFs singly deficient for either ATM or ligase IV (21). To date, the molecular mechanisms that underlie the synergistic effects of combined defects for ATM and various DNA repair factors have not been elucidated.

Atm and *H2ax* are very closely linked in both human and mouse and map to a cytogenetic region (11q23) often deleted in human cancers (22). Here, we have directly tested whether H2AX and ATM have synergistic functions in mouse development and maintenance of genomic stability by generating and analyzing H2AX and ATM double-deficient cells and mice. We find a dramatic synergy in both processes and implicate increased oxidative DNA damage associated with ATM deficiency, coupled with defective repair of this damage in the absence of H2AX, as an underlying mechanism.

Results and Discussion

Deficiency for Both H2AX and ATM Results in Midgestation Embryonic Lethality with Pleiotropic Developmental Defects. *H2ax* and *Atm* are located within 4 cm of each other on mouse chromosome 9. We

Author contributions: S.Z., C.H.B., and F.W.A. designed research; S.Z. and J.W.B. performed research; S.Z., J.S., and C.H.B. contributed new reagents/analytic tools; S.Z. analyzed data; and S.Z. and F.W.A. wrote the paper.

The authors declare no conflict of interest.

*Present address: Department of Internal Medicine, University of Michigan Comprehensive Cancer Center, University of Michigan Medical School, Ann Arbor, MI 48109.

†Present address: Department of Pathology and Laboratory Medicine, Center for Childhood Cancer Research, Children's Hospital of Philadelphia, University of Pennsylvania School of Medicine, Abramson Family Cancer Research Institute, Philadelphia, PA 19104.

‡To whom correspondence should be addressed at: Howard Hughes Medical Institute, Children's Hospital, 300 Longwood Avenue, Boston, MA 02115. E-mail: alt@enders.tch.harvard.edu.

This article contains supporting information online at www.pnas.org/cgi/content/full/0803520105/DCSupplemental.

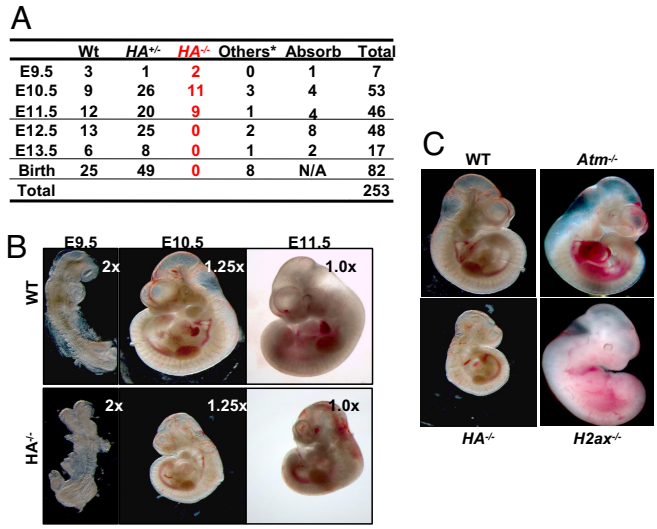

Fig. 1. *H2ax/Atm* double-deficient mice are embryonic lethal at E12.5. (*A*) Genotype of embryos obtained from timed breeding between $HA^{+/-}$ parental mice. The other genotypes include $H2ax^{+/-}$, $Atm^{+/-}$, $H2ax^{+/-}Atm^{-/-}$, and $H2ax^{-/-}Atm^{+/-}$ generated because of mitotic cross-over. (*B*) Morphology of representative E9.5, E10.5, and E11.5 WT and $HA^{-/-}$ embryos. The magnifications for the objective lenses used are marked at the upper right corner of each picture. (*C*) Morphology of representative E10.5 WT, $HA^{-/-}$, $Atm^{-/-}$, and $H2ax^{-/-}$ embryos. Right side view is shown. (Magnification, ×1.25.)

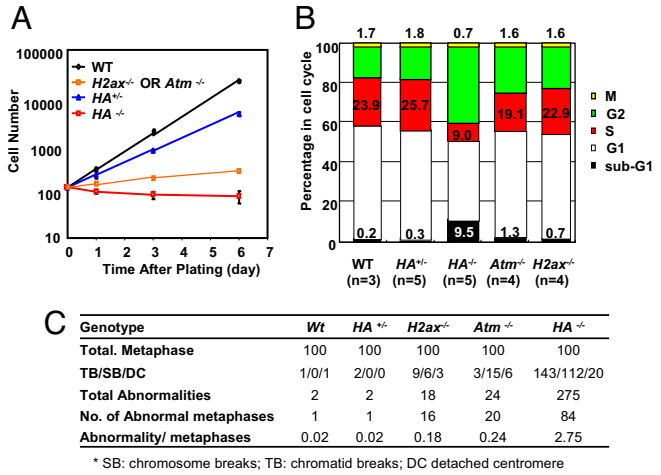

C

Genotype	*Wt*	*HA* +/-	*H2ax*-/-	*Atm* -/-	*HA* -/-
Total. Metaphase	100	100	100	100	100
TB/SB/DC	1/0/1	2/0/0	9/6/3	3/15/6	143/112/20
Total Abnormalities	2	2	18	24	275
No. of Abnormal metaphases	1	1	16	20	84
Abnormality/ metaphases	0.02	0.02	0.18	0.24	2.75

* SB: chromosome breaks; TB: chromatid breaks; DC detached centromere

Fig. 2. Proliferation defects and genomic instability in H2AX and ATM double deficient MEF. (*A*) Proliferation of *WT*, $HA^{-/-}$, $Atm^{-/-}$ and $H2ax^{-/-}$ MEFs. Approximately 2.5×10^2 P0 MEF were plated in each well of a 24 well plate at day 0, trypsinized and counted every other day by using trypan blue exclusion. The standard deviations are calculated based on the results from at least three independent experiments performed on independent MEF lines of each genotype. (*B*) Cell cycle analyses of overnight culture of p0 E10.5 MEF of indicated genotypes. The cells were incubated with BrdU and colcemid (100 ng/ml) for 2 h before collection for cell cycle assay. The sub-G_1, G_1, S, and G_2/M phase percentages were calculated from BrdU-PI staining. Mitotic cells were identified through histone H3 Ser-10-phosphorylation staining. G_2 phase percentage was obtained by subtracting the M phase percentage from the G_2/M phase percentage. The bar graphs represent the average of three to five independent MEF lines from each genotype. (*C*) Summary of cytogenetic analyses of p0 MEFs. DAPI staining was used to quantify the abnormalities.

bred mice heterozygous for an *H2ax*-inactivating mutation ($H^{+/-}$ mice; ref. 14) with mice heterozygous for an *Atm*-inactivating mutation ($A^{+/-}$ mice; ref. 2) to generate mice that carried the *H2ax*- and *Atm*-inactivating mutations on different chromosomes ($H^{+/-}A^{+/-}$ mice). $H^{+/-}A^{+/-}$ mice were crossed to wild-type (WT) mice to generate mice that carried the H^{-}- and A^{-}-inactivating mutations on the same chromosome ($HA^{+/-}$ mice), which were then crossed to obtain mice homozygous for the linked *H2ax*- and *Atm*-inactivating mutations [$HA^{-/-}$ mice; supporting information (SI) Fig. S1*A*]. Although $H^{-/-}$ and $A^{-/-}$ mice were born at expected Mendelian frequencies, no $HA^{-/-}$ pups were found in >100 pups analyzed, implying that H2AX and ATM have complementary roles required for mouse embryonic development (Fig. 1*A*).

The stage at which the development of $HA^{-/-}$ embryos arrests was determined from timed heterozygous crosses (Fig. 1*A*). At embryonic day 10.5 (E10.5), $HA^{-/-}$ embryos were alive, but smaller than WT littermates, $H^{-/-}$, and $A^{-/-}$ embryos (Fig. 1 *B* and *C*). $HA^{-/-}$ embryos had pleiotropic developmental defects (Fig. S1 *B* and *C*, and Fig. 1*D*), associated with increased cell death (Fig. S1*E*) and decreased mitotic index (Fig. S1*F*). Only 50% of E11.5 $HA^{-/-}$ embryos analyzed were alive, as judged by the presence of heartbeats, and no $HA^{-/-}$ embryos were detected at E12.5 (Fig. 1*A*). Thus, $HA^{-/-}$ embryos died between E11.5 and ≈12.5. Despite the severe defects of $HA^{-/-}$ embryos, $HA^{-/-}$ placentas had normal size, morphology, and structure (Fig. S1*G*), and $HA^{-/-}$ embryonic red blood cells were indistinguishable from those of WT littermates (Fig. S1*H*). Therefore, placental defects likely do not explain the embryonic lethality in $HA^{-/-}$ mice. Based on these and various other considerations (see below), we argue the embryonic lethality of $HA^{-/-}$ is likely caused by intrinsic defects in the embryonic cells.

H2AX and ATM Double-Deficient Embryonic Fibroblasts Have Dramatic Genomic Instability. To elucidate further potential causes of developmental failure in $HA^{-/-}$ mice, we derived E10.5 MEFs. E10.5 $H^{-/-}$ or $A^{-/-}$ MEFs proliferated *in vitro*, albeit more slowly than WT MEFs (Fig. 2*A*), similar to what has previously been reported for E13.5 MEFs from these genetic backgrounds (1, 13). In contrast, total cell numbers of p0 $HA^{-/-}$ MEFs decreased during culture, implying continued cell death even in freshly isolated MEFs (Fig. 2*A*). Cell cycle analyses of p0 $HA^{-/-}$ MEF cultures revealed a dramatic increase in the sub-G_1 population, indicative of massive cell death (Fig. 2*B*). Cell cycle analyses of p0 $HA^{-/-}$ MEFs also revealed a significantly decreased fraction of cells in S phase and a corresponding increase in relative cell numbers in the G_1 and G_2 fractions (Fig. 2*B*), a cell cycle distribution that has been observed in irradiated WT MEFs that harbor a high level of genomic instability (23). Therefore, we assayed p0 $HA^{-/-}$ MEFs for potential genomic instability. Although only 2–3% of WT or $HA^{+/-}$ and 18–25% of $H^{-/-}$ or $A^{-/-}$ metaphases had cytogenetic aberrations, ≈80% of $HA^{-/-}$ metaphases showed cytogenetic aberrations (Fig. 2*C*). Furthermore, most of the $HA^{-/-}$ metaphases contained numerous breaks per metaphase (average more than three abnormalities per abnormal metaphase), in contrast to one or, rarely, two aberrations per abnormal metaphase observed in $H^{-/-}$ or $A^{-/-}$ MEFs (Fig. 2*C*). Thus, the severe proliferation defects of $HA^{-/-}$ MEFs are associated with severe genomic instability, which may be a basis for the observed embryonic lethality of $HA^{-/-}$ mice.

H2AX and ATM Double-Deficient Embryonic Stem (ES) Cells Have Dramatic Genomic Instability. To explore the effect of loss of H2AX and ATM on genomic instability in other cell types, we generated H2AX/ATM double-deficient ES cells. We used conditionally targeted alleles for each gene to avoid potential adverse effects of sequentially inactivating *H2ax* and *Atm* in cells. We used the *H2ax* conditional allele previously generated in our laboratory (24). We generated an *Atm* conditional targeting allele by flanking exons 57 and 58 of *Atm* gene, which encode the core PIKK kinase domain of murine *Atm*, with two *loxP* sites (Fig. 3 *A* and *B*). Cre-dependent removal of exons 57 and 58 of

GENETICS

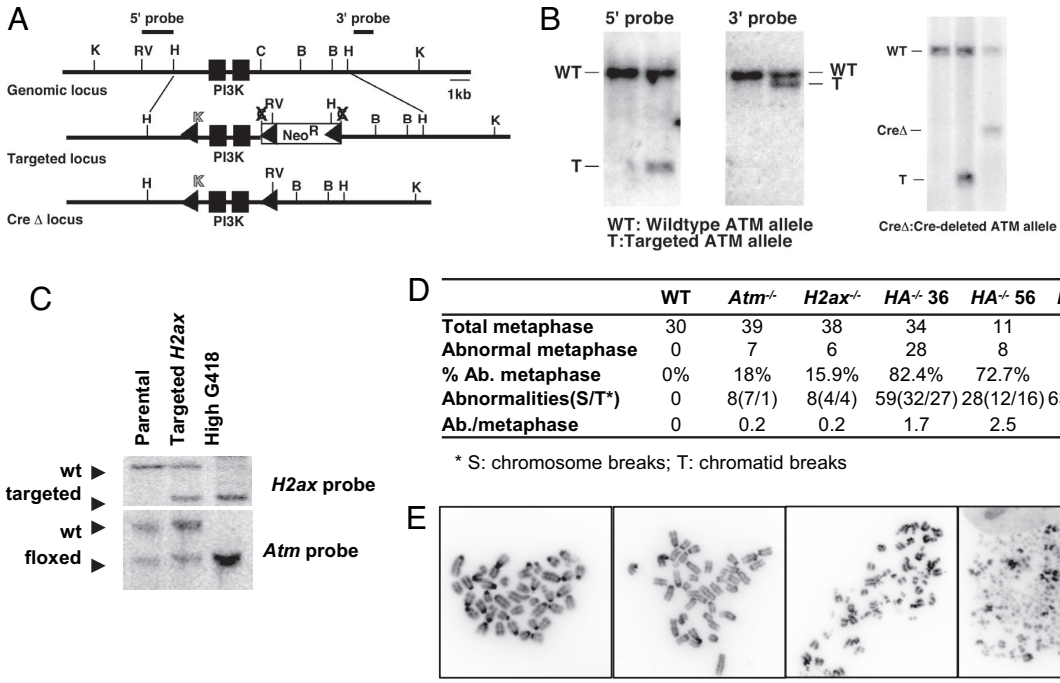

	WT	*Atm*$^{-/-}$	*H2ax*$^{-/-}$	*HA*$^{-/-}$ 36	*HA*$^{-/-}$ 56	*HA*$^{-/-}$ 59
Total metaphase	30	39	38	34	11	57
Abnormal metaphase	0	7	6	28	8	44
% Ab. metaphase	0%	18%	15.9%	82.4%	72.7%	77.2%
Abnormalities(S/T*)	0	8(7/1)	8(4/4)	59(32/27)	28(12/16)	63(25/38)
Ab./metaphase	0	0.2	0.2	1.7	2.5	1.1

* S: chromosome breaks; T: chromatid breaks

Fig. 3. Generation and characterization of H2AX and ATM double-deficient ES cells. (*A*) Schematic diagram of mouse *Atm* genomic locus, *Atm* conditional targeting vector, and targeted *Atm* conditional target allele. Restriction site designations: K, KpnI; B, BamHI; H, HindIII; C, ClaI; RV, EcoRV. (*B*) Southern blot analysis of WT (left lane), *Atm*-targeted allele (second lane) and *Atm*$^{\Delta}$ allele (third lane). (*C*) Southern blot analysis *of H2ax and Atm* locus of parental Atm$^{+/c}$ ES cells, *H2ax*$^{+/Neo}$ *Atm*$^{+/C}$-targeted ES cells, and *H2ax*$^{Neo/Neo}$*Atm*$^{C/C}$ HighG418-selected clone. (*D*) Summary of cytogenetic analyses of *WT*, *HA*$^{-/-}$, *Atm*$^{-/-}$, and *H2ax*$^{-/-}$ ES cells. Three independent clones of *HA*$^{-/-}$ ES cells were analyzed. Cytogenetic abnormalities were quantified with DAPI staining. Only metaphases with countable abnormalities (n <10) were quantified. (*E*) Representative metaphases from *HA*$^{-/-}$ ES cells with different levels of genomic instability.

the *Atm* gene on the A^c allele generates an A^{Δ} allele that is similar to a previously published *Atm*-null allele (Fig. 3 *A* and *B*) (25) and led to the generation of $A^{\Delta/\Delta}$ ES cells that are identical to previously characterized *Atm*$^{-/-}$ cells in all phenotypic aspects (data not shown). We then generated *HA*$^{-/-}$ ES cells through sequential targeting and high G418 selection (26) (Fig. 3*C*). Although proliferation of $H^{-/-}$ or $A^{-/-}$ ES cells was indistinguishable from that of WT ES cells, *HA*$^{-/-}$ ES cells grew poorly and exhibited frequent cell death (data not shown).

Metaphase analyses of three independent clones showed that >70% of *HA*$^{-/-}$ ES cells exhibited cytogenetic abnormalities (Fig. 3*D*), ranging from mild (<10 cytogenetic abnormalities per metaphase; Fig. 3*E Left two panels*) to extensive (e.g., major chromosomal fragmentation occurred in ≈10% of metaphases Fig. 3*E Right two panels*). Notably, the general genomic instability in *HA*$^{-/-}$ ES cells (only breaks from metaphases with mild genomic instability were counted and categorized) was approximately evenly distributed between chromosome and chromatid breaks, a pattern similar to that observed in $H^{-/-}$ ES cells but different from that of $A^{-/-}$ ES cells, which show mainly chromosome breaks (Figs. 3*D* and 4*D*). Together, these results indicate that H2AX and ATM synergistically suppress general genomic instability both before and after DNA replication, even though ATM deficiency alone leads to chromosomal anomalies that reflect damage generated in prereplicative stages. We also used the conditionally targeted *Atm* and *H2ax* alleles to generate mature B and T cells that lacked both ATM and H2AX, and we found them to have similarly increased genomic instability, compared with B cells deficient for ATM or H2AX alone (data not shown). Thus, the synergistic functions of these proteins in maintaining genomic stability are not limited to embryonic cell types.

Increased ROS-Induced DNA Damage and Decreased Repair Lead to Increased Genomic Instability in *HA*$^{-/-}$ Cells. Because ATM-deficient cells have increased intracellular ROS (5), we asked whether *HA*$^{-/-}$ cells also had increased ROS. We measured intracellular ROS in *HA*$^{-/-}$ ES cells by using 2′,7′-dichlorfluorescein-diacetate (DFC), which is converted to a fluorophore upon exposure to free radicals (5). ROS levels in *HA*$^{-/-}$ ES cells were similar to those in $A^{-/-}$ cells and significantly higher than those in WT or $H^{-/-}$ ES cells (Fig. 4*A Upper*). To test whether H2AX deficiency confers hypersensitivity to increased oxidative stress, we exposed $H^{-/-}$ ES cells to different levels of H_2O_2 in parallel with WT ES cells. Although 25 μM H_2O_2 had no significant impact on WT cells, it caused a 50% decrease in the number of colonies from $H^{-/-}$ ES cells (Fig. 4*B*). Thus, $H^{-/-}$ ES cells are hypersensitive to H_2O_2, indicating that H2AX is required for the repair of ROS-induced DNA damage. Together, these findings support the notion that H2AX deficiency may lead to hypersensitivity to the high cellular ROS levels associated with ATM deficiency and, thereby, cause the proliferation defects of *HA*$^{-/-}$ cells. We note that ES cells deficient for either H2AX or ATM alone have similar genomic instability, even though H2AX-deficient ES cells lack the elevated ROS levels observed in ATM-deficient ES cells, suggesting that the ROS defect associated with ATM deficiency is not necessarily caused by a DNA repair defect *per se*. However, current studies have not excluded a role for a DSB repair defect in the generation of increased ROS found in the context of ATM deficiency (7). To elucidate further the relationship between increased ROS and DNA repair, it would be of interest to measure ROS levels in other DNA repair-deficient cells, including nonhomologous end joining (NHEJ)-deficient cells.

To test whether ROS hypersensitivity of $H^{-/-}$ ES cells leads to genomic instability, we treated these cells with 100 μM H_2O_2 for 24 h and analyzed metaphase spreads. Indeed, we observed markedly increased cytogenetic abnormalities in H_2O_2-treated $H^{-/-}$ ES cells (15% ± 1.7% before H_2O_2 treatment and 41% ± 5.1% after H_2O_2 treatment; $P < 0.01$, Fig. 4*C Left*), compared

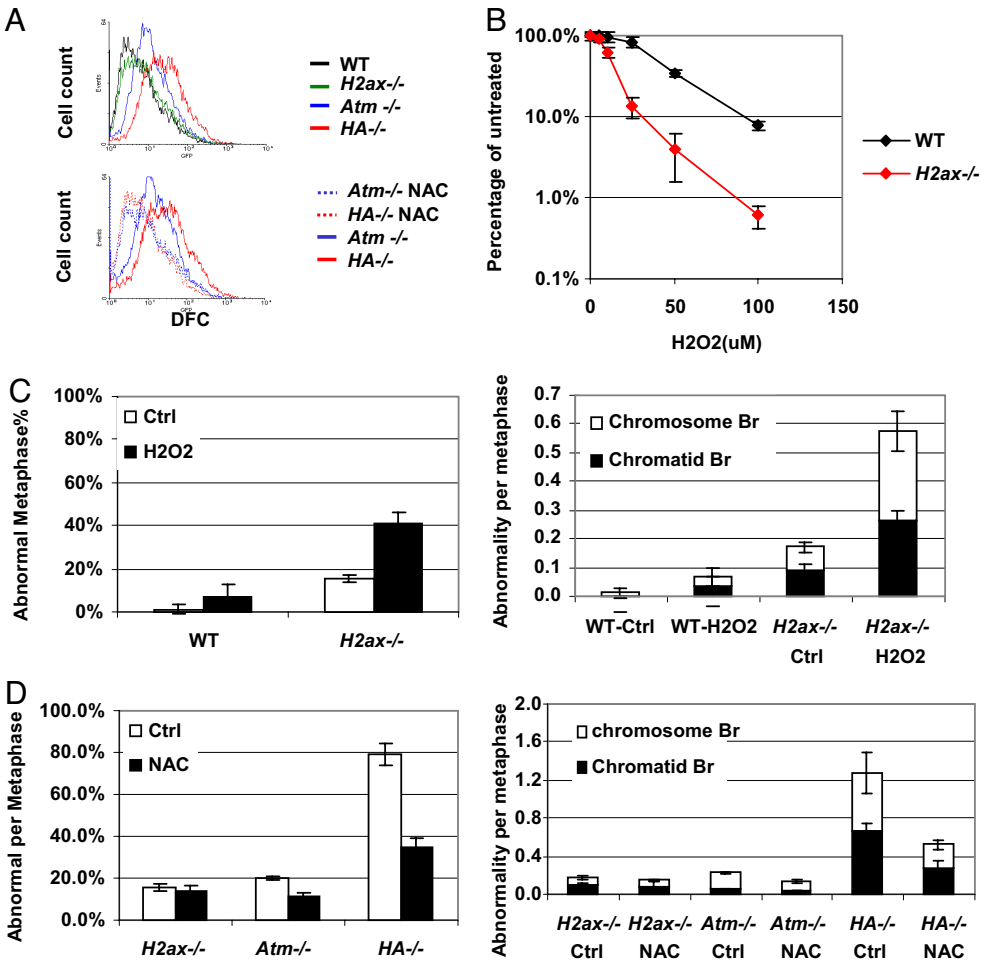

Fig. 4. Elevated ROS levels contribute to the severe genomic instability in *H2ax/Atm* double-deficient ES cells. (*A*) Intracellular ROS levels from WT, $H2ax^{-/-}$, $Atm^{-/-}$, $HA^{-/-}$ ES cells, and cells treated with NAC (1 mM for 96 h) measured by DFC-mediated fluorescence. (*B*) H_2O_2 sensitivity of WT and $H2ax^{-/-}$ ES cells. The percentages of surviving colonies after 7-day culture were plotted as the function of H_2O_2 concentration. Each data point represents the average of three independent experiments performed on at least two independent ES lines of each genotype. (*C*) Percentage of abnormal metaphases (*Left*) and average cytogenetic abnormalities per metaphase (*Right*) for WT and $H2ax^{-/-}$ ES cells treated with 100 μM H_2O_2 for 24 h. (*D*) Percentage of abnormal metaphases (*Left*) and cytogenetic abnormalities per metaphase (*Right*) for $H2ax^{-/-}$, $Atm^{-/-}$, and $HA^{-/-}$ ES cells treated with 1 mM NAC for at least 96 h.

with H_2O_2-treated WT cells (1.1% ± 1.9% before H_2O_2 and 6.7% ± 5.8% after H_2O_2 treatment; $P > 0.1$, Fig. 4*C Left*). Treatment with *N*-acetyl-L-cysteine (NAC), a ROS scavenger, had no significant impact on the level of genomic instability in $H^{-/-}$ ES cells (15.3% ± 1.7% before NAC treatment and 13.6% ± 3.2% after NAC treatment; $P > 0.1$, Fig. 4*D Left*). However, NAC treatment significantly decreased spontaneous genomic instability in $HA^{-/-}$ ES cells (from 79.2% ± 5.3% to 35.5%% ± 7.3% abnormal metaphases; $P < 0.01$, Fig. 4*D Left*), in association with a corresponding reduction in intracellular ROS levels (Fig. 4*A Lower*). Notably, chromosomal abnormalities in H_2O_2-treated $H^{-/-}$ cells, like those observed in untreated $HA^{-/-}$ cells (Figs. 3*D* and 4*D Right*), were evenly distributed into chromosome and chromatid breaks (Fig. 4*C Right*). Together, these results indicate that a significant proportion of the DNA lesions caused by elevated ROS levels in ATM-deficient cells are repaired in an H2AX-dependent fashion. Thus, the absence of both ATM and H2AX leads to greatly increased levels of genomic instability compared with levels found in the context of either ATM or H2AX deficiency alone. In addition, our findings further implicate this mechanism as leading to severe proliferation defects of $HA^{-/-}$ cells compared with $H^{-/-}$ or $A^{-/-}$ cells and, by extension, they suggest that this mechanism is a major contributing factor to the embryonic lethality of $HA^{-/-}$ mice. We note that NAC treatment did not completely eliminate genomic instability in $A^{-/-}$ or $HA^{-/-}$ ES cells. In this regard, incomplete rescue may simply reflect the inability of NAC to completely rescue all ROS, including species not detected by the DFC assay (which detects mainly H_2O_2). However, it remains possible that ROS-independent mechanisms, such as ATM-independent repair functions of H2AX downstream of other PIKK family members, might also contribute to the synergistic genomic instability in $HA^{-/-}$ cells.

Additional Implications. Our studies demonstrate that elevated ROS leads to chromosomal instability in ATM-deficient cells and further show that H2AX is required for the repair of ROS-induced DNA damage in ATM-deficient cells. In addition, we note that H2AX/ATM double-deficient cells have only a modest increase in chromosome breaks compared with ATM-deficient cells, suggesting that H2AX and ATM have significantly overlapping functions in the repair of G_1 phase DSBs (Fig. 4 *C* and *D*). In contrast, H2AX and ATM double-deficient cells had a much more substantial increase in chromatid breaks (Fig. 3 *C* and *D*), consistent with ATM-independent repair functions of H2AX in postreplicative cell cycle phases (Fig. 3 *C* and *D*). It

remains unknown what kinase, if any, is responsible for postreplicative DSB repair upstream of H2AX. Although both ATR and DNA-PKcs have been implicated (16–18), DNA-PKcs deficiency does not lead to a significant level of chromatid breaks (27). However, redundancy among ATM, DNA-PKcs, and ATR in the postreplicative DSB response has not been ruled out. ATM deficiency also leads to substantially increased genomic instability and growth defects in ligase IV- and PARP1/2-deficient cells (20, 21). Although the mechanism by which deficiencies for these factors impacts on ATM-deficient cells is not known, deficiencies for PARP1/2 or NHEJ have both been linked to hypersensitivity to H_2O_2 (28, 29). Therefore, based on our findings with H2AX/ATM double-deficient cells, it is tempting to speculate that the elevated ROS levels associated with ATM deficiency might underlie at least a portion of the observed increases in genomic instability and the severe growth defects of PARP1/2- or ligase IV-deficient cells also deficient for ATM.

Experimental Procedures

ES Cell Targeting. The ATM conditional targeting vector was constructed from pLNTK (30) and was designed to flank the core PIKK kinase domain coding exons (exon 57 and 58) with loxP sites (Fig. 3*A*). The 5′ homology arm was a 4.5-kb HindIII/ClaI fragment with a KpnI site and a loxP site next to each other inserted into a BstAPI sites. The 3′ homology arm was a 3.0-kb HindIII/ClaI fragment. The 5′ ATM probe was the 1.5-kb EcoRV/HindIII fragment immediately upstream of the 5′ homology arm. The 3′ ATM probe was a 635-bp fragment generated by PCR using primers 5′-GGCATCTGCTTGACTGCAGTAAATCAGGCGG-3′ and 5′-GGGGTACTGCAGCATAGGGCTGGAAGAGG-3′ (Fig. 3*A*). The targeting construct was electroporated into TC1 ES cells, and targeted clones were identified by Southern blotting with the 3′ ATM probe on EcoRV-digested DNA (17-kb ATM^{Neo}, 22-kb ATM^{WT}) and confirmed with the 5′ ATM probe on EcoRV-digested DNA (7-kb ATM^{Neo}, 22-kb ATM^{WT}) and the 3′ probe on KpnI-digested DNA to detect integration of the 5′ *loxP* site (12 kb). The PGK-*neo*^{r} gene cassette was removed by infection with adenovirus carrying Cre recombinase. The resulted $ATM^{+/c}$ and $ATM^{+/\Delta}$ clones were identified and confirmed with 3′ ATM probe on KpnI digestion (16-kb ATM^{WT}, 12-kb ATM^{Neo}, 10-kb ATM^{c}, 12-kb ATM^{Δ}) and with 5′ ATM probe on the same KpnI digestion (16-kb ATM^{WT}, 5.3-kb ATM^{Neo}, 5.3-kb ATM^{c}, 12-kb ATM^{Δ}) (Fig. 3 *A* and *B*).

To generate the *H2ax*/*Atm* double-deficient ES cells, H2AX targeting vector was electroporated into $ATM^{+/c}$ ES cells, and the correct targeting was confirmed by Southern blot analyses as described before (Fig. 3*C*) (24). Then, high-G418 selections were conducted on multiple independent $ATM^{+/c}H2AX^{+/Neo}$ ES clones to induce duplication of the neo-containing chromosome and the loss of the other corresponding allele (26). Two independent $ATM^{Flox/Flox}H2AX^{Neo/Neo}$ ES clones were identified by Southern blotting (Fig. 3*C*) and subjected to adenovirus-mediated Cre deletion to obtain $ATM^{\Delta/\Delta}H2AX^{-/-}$ ($HA^{-/-}$)ES cells.

Proliferation and Cytogenetic Analysis for MEF. E10.5 MEF cells were isolated from breeding of $HA^{+/-}$, $A^{+/-}$, or $H^{+/-}$ mice. Proliferation assay and cell cycle analysis were performed on p0 MEF as described in ref. 29. For cytogenetic analysis, colcemid (final concentration of 100 ng/ml) was added directly to overnight-cultured p0 MEF for 5 h, and metaphase were collected as described before in ref. 29. DAPI staining was used to quantify the cytogenetic abnormalities. Detached centromere is scored as chromosome breaks in Fig. 3 *C* and *D*.

ACKNOWLEDGMENTS. We thank Dr. Sonia Franco for technical advice on cytogenetic analyses. We also thank Tiffany Borjeson, Nicole Stokes, and Yuko Fujiwara for helps on ES cell injections, mouse breeding, and genotyping. This work was supported by National Institutes of Health Grants 5P01 CA92625-06 and 5P01 CA109901-03 (to F.W.A.) and 5R01 CA125195-02 (to C.H.B.). S.Z. was a Fellow and now a Senior Fellow of the Leukemia and Lymphoma Society. C.H.B. is a Pew Scholar in the Biomedical Sciences. J.S. was a Senior Fellow of Leukemia and Lymphoma Society and is a Pew Scholar in the Biomedical Sciences. F.W.A. is a Howard Hughes Medical Institute investigator.

1. Barlow C, *et al*. (1996) Atm-deficient mice: A paradigm of ataxia–telangiectasia. *Cell* 86:159–171.
2. Borghesani PR, *et al*. (2000) Abnormal development of Purkinje cells and lymphocytes in Atm mutant mice. *Proc Natl Acad Sci USA* 97:3336–3341.
3. Elson A, *et al*. (1996) Pleiotropic defects in ataxia–telangiectasia protein-deficient mice. *Proc Natl Acad Sci USA* 93:13084–13089.
4. Herzog KH, Chong MJ, Kapsetaki M, Morgan JI, McKinnon PJ (1998) Requirement for Atm in ionizing radiation-induced cell death in the developing central nervous system. *Science* 280:1089–1091.
5. Ito K, *et al*. (2004) Regulation of oxidative stress by ATM is required for self-renewal of haematopoietic stem cells. *Nature* 431:997–1002.
6. Ito K, *et al*. (2006) Reactive oxygen species act through p38 MAPK to limit the lifespan of hematopoietic stem cells. *Nat Med* 12:446–451.
7. Barzilai A, *et al*. (2002) ATM deficiency and oxidative stress: A new dimension of defective response to DNA damage. *DNA Repair* 1:3–25.
8. Ito K, *et al*. (2007) Regulation of reactive oxygen species by Atm is essential for proper response to DNA double-strand breaks in lymphocytes. *J Immunol* 178:103–110.
9. Schubert R, *et al*. (2004) Cancer chemoprevention by the antioxidant tempol in Atm-deficient mice. *Hum Mol Genet* 13:1793–1802.
10. Rogakou EP, *et al*. (1999) Megabase chromatin domains involved in DNA double-strand breaks *in vivo*. *J Cell Biol* 146:905–916.
11. Bassing CH, Alt FW (2004) The cellular response to general and programmed DNA double strand breaks. *DNA Repair* 3:781–796.
12. Lou Z, *et al*. (2006) MDC1 maintains genomic stability by participating in the amplification of ATM-dependent DNA damage signals. *Mol Cell* 21:187–200.
13. Celeste A, *et al*. (2002) Genomic instability in mice lacking histone H2AX. *Science* 296:922–927.
14. Bassing CH, *et al*. (2003) Histone H2AX: A dosage-dependent suppressor of oncogenic translocations and tumors. *Cell* 114:359–370.
15. Celeste A, *et al*. (2003) H2AX haploinsufficiency modifies genomic stability and tumor susceptibility. *Cell* 114:371–383.
16. Furuta T, *et al*. (2003) Phosphorylation of histone H2AX and activation of Mre11, Rad50, and Nbs1 in response to replication-dependent DNA double-strand breaks induced by mammalian DNA topoisomerase I cleavage complexes. *J Biol Chem* 278:20303–20312.
17. Stiff T, *et al*. (2004) ATM and DNA-PK function redundantly to phosphorylate H2AX after exposure to ionizing radiation. *Cancer Res* 64:2390–2396.
18. Ward IM, Chen J (2001) Histone H2AX is phosphorylated in an ATR-dependent manner in response to replicational stress. *J Biol Chem* 276:47759–47762.
19. Franco S, *et al*. (2006) H2AX prevents DNA breaks from progressing to chromosome breaks and translocations. *Mol Cell* 21:201–214.
20. Huber A, Bai P, de Murcia JM, de Murcia G (2004) PARP-1, PARP-2, and ATM in the DNA damage response: Functional synergy in mouse development. *DNA Repair* 3:1103–1108.
21. Sekiguchi J, *et al*. (2001) Genetic interactions between ATM and the nonhomologous end-joining factors in genomic stability and development. *Proc Natl Acad Sci USA* 98:3243–3248.
22. Monni O, Knuutila S (2001) 11q deletions in hematological malignancies. *Leuk Lymphoma* 40:259–266.
23. Xu B, Kim ST, Lim DS, Kastan MB (2002) Two molecularly distinct G_2/M checkpoints are induced by ionizing irradiation. *Mol Cell Biol* 22:1049–1059.
24. Bassing CH, *et al*. (2002) Increased ionizing radiation sensitivity and genomic instability in the absence of histone H2AX. *Proc Natl Acad Sci USA* 99:8173–8178.
25. Xu Y, *et al*. (1996) Targeted disruption of ATM leads to growth retardation, chromosomal fragmentation during meiosis, immune defects, and thymic lymphoma. *Genes Dev* 10:2411–2422.
26. Mortensen RM, Conner DA, Chao S, Geisterfer-Lowrance AA, Seidman JG (1992) Production of homozygous mutant ES cells with a single targeting construct. *Mol Cell Biol* 12:2391–2395.
27. Franco S, et al. (2008) DNA-PKcs and Artemis function in the end-joining phase of immunoglobulin heavy chain class switch recombination. *J Exp Med* 205:557–564.
28. David SS, O'Shea VL, Kundu S (2007) Base-excision repair of oxidative DNA damage. *Nature* 447, 941–950.
29. Mostoslavsky R, *et al*. (2006) Genomic instability and aging-like phenotype in the absence of mammalian SIRT6. *Cell* 124:315–329.
30. Gorman JR, *et al*. (1996) The Igκ enhancer influences the ratio of Igκ versus Igλ B lymphocytes. *Immunity* 5:241–252.